



Photocatalytic degradation of deoxynivalenol using graphene/ZnO hybrids in aqueous suspension



Xiaojuan Bai^{a,*}, Changpo Sun^{a,*}, Di Liu^b, Xiaohong Luo^a, Di Li^c, Jun Wang^a, Nanxi Wang^a, Xiaojiao Chang^a, Ruilong Zong^d, Yongfa Zhu^d

^a Academy of State Administration of Grain P.R.C, No. 11 Baiwanzhuang Avenue, Xicheng District, Beijing 100037, China

^b School of Chemical & Environmental Engineering, China University of Mining & Technology, Ding No.11 Xueyuan Road, Haidian District, Beijing 100083, China

^c School of Metallurgical Engineering, Xi'an University of Architecture and Technology, Xi'an 710055, China

^d Department of Chemistry, Tsinghua University, Beijing 100084, China

ARTICLE INFO

Article history:

Received 26 September 2016

Received in revised form 18 October 2016

Accepted 7 November 2016

Available online 11 November 2016

Keywords:

Photocatalysis

ZnO

Graphene

Hybridization

Deoxynivalenol

ABSTRACT

Water-soluble deoxynivalenol (DON) pose a major threat as a potential organic pollutant to water environmental quality. DON is a toxic secondary metabolite produced by molds of the Fusarium genus and one of the most important mycotoxins in cereal commodities, which can be enriched from the contaminated grain by deoxynivalenol in the process of wet processing. In this work, graphene/ZnO hybrids has been successfully prepared via a simple one-step hydrothermal method and exhibited superior photocatalytic activity for the photodegradation of DON under the irradiation of UV light. The UV light photocatalytic activity of graphene/ZnO hybrid GZ0.3 was 3.1 times than pure ZnO and about 99% of DON (15 ppm) could be photodegraded within 30 min totally while there were three peaks of intermediate products appeared. The ESI/MS analysis confirmed the presence of DON and degradation product with the secondary mass spectrogram in the positive ESI mode. Overall, this work could provide new insights into the fabrication of graphene/ZnO hybrids composite as high performance photocatalysts and facilitate their application in the mycotoxin detoxification and environmental protection issues.

© 2016 Elsevier B.V. All rights reserved.

1. Introduction

Water-soluble deoxynivalenol pose a major threat as a potential organic pollutant to water environmental quality. In the process of wet processing, soluble-toxin molecules can be enriched from the contaminated grain by deoxynivalenol, which will pose a potentially serious threat to water environment. Deoxynivalenol belongs to trichothecenes which are a group of over 180 structurally related sesquiterpenoid mycotoxins produced mainly by Fusarium species growing on basic commodities including wheat, maize and barley [1,2]. The group is subdivided in type A trichothecenes such as T-2 toxin and type B trichothecenes such as deoxynivalenol, the difference being a keto substitution at C-8 in the latter case (Fig. S1) [3]. Although type B trichothecenes are generally less acutely toxic than type A-, C-, and D-trichothecenes,

they are the most prevalent congeners in grain [4]. DON possesses structural and toxicity features that may give rise to chemical reactivity—the epoxyring, hydroxyl groups, and an α,β -unsaturated carbonyl group [5,6]. Bretz et al. reported that the stability of DON under food-processing conditions such as cooking or baking and performed model heating experiments to screen the residue for degradation products. They found that heating of DON and 3-acetyldeoxynivalenol (3-AcDON) can give a mixture of compounds under alkaline conditions and reduce the toxicity of DON [3]. Park et al. investigated the degradation of three different mycotoxins, aflatoxin B1 (AFB1), deoxynivalenol (DON) and nivalenol (NIV) by using our self-designed microwave-induced argon plasma system at atmospheric pressure. The mycotoxins AFB1, DON, and NIV were completely removed after 5 s of plasma treatment and the cytotoxicity of mycotoxins was significantly reduced with the progress in the treatment time [7]. The γ -irradiation of AFB1 was reported to have encouraging degradation rates in several studies [8–11], and the identification of radiolytic products and the confirmation of toxicity have been studied by Wang et al. group [12]. Mishra et al. studied influence of temperature and pH on the degradation of deoxynivalenol (DON) in aqueous medium and the results suggest that standard DON was unstable at 125–250 °C showing 16–100%

* Corresponding authors.

E-mail addresses: heixia.1986@163.com
(X. Bai), chpsun@163.com (C. Sun), liudi0713@163.com (D. Liu), lxh@chinagrain.org
(X. Luo), lid180315@163.com (D. Li), wj2010922@126.com (J. Wang),
wangnanxi2003@163.com (N. Wang), cxi.jj@hotmail.com (X. Chang),
zrl01@mails.tsinghua.edu.cn (R. Zong), zhuyf@tsinghua.edu.cn (Y. Zhu).

degradation whereas DON at pH 1–3 had 30–66% degradation, with a concomitant increase in the formation of a degraded product [13]. Wu et al. performed systematic studies of a range of physicochemical parameters, such as temperature, moisture, compression, residence time in the extruder, pH value, and protein content, and it was shown that the reduction of deoxynivalenol levels is dependent on a set of parameters partially interacting with each other during extrusion cooking [14]. To date, although numerous conventional physical, chemical and biological detoxification methods have been tested, none really fulfills the necessary efficacy and safety. Meanwhile, the degradation effect is limited and mechanism is still not clear, which needs further investigated deeply. Therefore, the development of a green and efficient detoxification technology is essential to improve the efficiency of decontamination of soluble deoxynivalenol and reduce treatment cost [15,16].

The photocatalytic degradation technology is gaining importance in the area of pollutants treatment, especially for wastewater containing small amounts of refractory organic substances, which could be applied for mycotoxin detoxification. The technology has several advantages over competing methods. These are: (1) complete mineralization, (2) no waste disposal problem, (3) low cost, and (4) only mild temperature and pressure conditions are necessary [17]. Although photocatalytic technology showed great potential for degradation of organic pollutants, it is still challenging to obtain high photocatalytic efficiency. Recombination of photoinduced charge is a key barrier for quantum efficiency of photocatalysis [18]. Therefore, there is a great demand for a novel approach to promote the photocatalytic efficiency by decreasing the recombination rate. Graphene sheets (GS), excellent electron collectors and transporters, have been used to boost performance of various energy conversion and storage devices such as photovoltaic devices, supercapacitors, fuel cells, and Li-ion batteries [19–24]. ZnO semiconductor is an important photocatalyst due to its nontoxic nature, low cost, and high reactivity. It has been widely used in degradation of environmental pollutants in air or water, as well as transformation selective organic pollutants to nontoxic small molecule even to CO₂/H₂O [25,26]. Recently, functionalized graphene-based semiconductor photocatalysts have attracted a lot of attention due to their good electron conductivity, large specific surface area and high adsorption [20]. Although it has been shown previously that the graphene-based semiconductor exhibited enhanced photocatalytic performance than pure photocatalyst alone, some problems still hinder further application of the present nanocomposites.

In this work, it is the first time to demonstrate the graphene/ZnO hybrid photocatalysts can be used to detoxification of DON in aqueous suspension and the probable structure of intermediate product is investigated as well as the influence of graphene on the photocatalytic activity for DON degradation has been elucidated systematically. Furthermore, the UV (254 nm, 365 nm) light activity of ZnO for photodegradation of DON was enhanced after graphene surface hybridization. It was shown that the photocatalytic activity of ZnO/graphene hybrid for DON degradation is dependent on the content of graphene and exhibited stable efficiency toward the DON photodegradation for an extended period of time. The photocatalytic activity and intermediate product for DON degradation may provide new insight for green and efficient detoxification technology to improve the efficiency of decontamination of mycotoxins and reduce treatment cost.

2. Experimental section

2.1. Materials

Graphite powder (325 mesh) were purchased from Qingdao Huatai Lubricant Sealing S&T Co. Ltd., Qingdao, China. Acetonitrile

and methanol of HPLC grade were obtained from Honeywell Co. Ltd. ZnO nanopowder (particle diameter 10–20 nm, surface area 10.4 m² g⁻¹) were commercially available. Water used in the work was purified with a Milli-Q system (Millipore, Billerica, MA). Potassium permanganate (KMnO₄), hydrochloric acid (HCl), sulfuric acid (H₂SO₄, 98%), hydrogen peroxide (H₂O₂, 30%), phosphoric acid (H₃PO₄, 85%) and trifluoroacetic acid (TFA) were from Sinopharm Chemical Reagent Co. Ltd. (Shanghai, China). All the chemicals and solvents were of analytical grade except acetonitrile and methanol, which were of HPLC grade. DON standard was purchased from Sigma-Aldrich (St. Louis, MO, USA). All the standard solutions were stored in the dark at 4 °C.

2.2. Synthesis of graphene oxide

Graphene oxide was prepared by oxidation of natural graphite powder according to the modified Hummers' method [27]. Briefly, graphite (3.0 g) was added to concentrated sulfuric acid (70 mL) under stirring at room temperature, then sodium nitrate (1.5 g) was added, and the mixture was cooled to 0 °C. Under vigorous agitation, potassium permanganate (9.0 g) was added slowly to keep the temperature of the suspension lower than 20 °C. Successively, the reaction system was transferred to a 35–40 °C water bath for about 0.5 h, forming a thick paste. Then, 140 mL of water was added, and the solution was stirred for another 15 min. An additional 500 mL of water was added followed by a slow addition of 20 mL of H₂O₂ (30%), turning the color of the solution from brown to yellow. The mixture was filtered and washed with 1:10 HCl aqueous solution (250 mL) to remove metal ions followed by repeated washing with water and centrifugation to remove the acid. The resulting solid was dispersed in water by ultrasonication for 1 h to make a graphene oxide aqueous dispersion (0.5 wt%). The obtained brown dispersion was then subjected to 30 min of centrifugation at 4000 rpm to remove any aggregates. Finally, it was purified by dialysis for 1 week to remove the remaining salt impurities for the following experiments.

2.3. Preparation of graphene-ZnO hybrid photocatalyst

The graphene/ZnO hybrids were synthesized and the detail process as follows: Appropriate GO was well dispersed in distilled water, and then the dispersion was ultrasonicated for 60 min to get GO exfoliated. The obtained brown dispersion was then subjected to 30 min of centrifugation at low speed 5000 rpm to remove any unexfoliated GO. Subsequently, the suspension was then centrifuged at high speed 10,000 rpm to remove the residual supernatant. The obtained exfoliated GO was then dispersed in 100 mL of water, and certain amount of pure ZnO was added into the GO dispersion, respectively. The ZnO nanoparticles and GO mixture was dispersed by ultrasonication for 30 min and stirred for 3 h and then homogeneous mixture dispersion was sealed in a 16 mL Teflon-lined autoclave and maintained at 180 °C for 6 h. Then the autoclave was naturally cooled to room temperature and the as-prepared samples were taken out, washed with deionized water and ethanol in turn to remove surface impurities for following experiments. The graphene oxide content in the composite was tuned by changing the amount of the added graphite oxide. The graphene/ZnO hybrids with different mass ratio of graphene from 0.1% to 10.0% were prepared according to above method. The graphene/ZnO-X wt% hybrid photocatalysts were marked as GZX, X label as graphene/ZnO hybrids mass ratio 0.1, 0.3, 3.0, 5.0, 8.0, and 10.0.

2.4. Characterizations

The samples were characterized by powder X-ray diffraction (XRD) on a Bruker D8-advance X-ray diffractometer at 40 kV and 40 mA for monochromatized Cu K α ($\lambda = 1.5406 \text{ \AA}$) radiation. The Brunauer–Emmett–Teller (BET) specific surface area of the samples was characterized by nitrogen adsorption at 77 K with a Micromeritics 3020 instrument. Zeta potential measurements were made with a Delsa Nano C zeta potential instrument (Beckman Coulter). The morphologies and sizes of the as-prepared products were examined through a LEO-1530 field emission Scanning Electron Microscope (SEM) and a HITACHI HT7700 transmission electron microscope (TEM). Fourier transform infrared spectra (FT-IR) were taken with a Bruker VERTEX 700 spectrometer in the frequency range of 4000–600 cm $^{-1}$ with a resolution of 4 cm $^{-1}$. The diffuse reflectance absorption spectra (DRS) of the samples were recorded in the range from 250 to 800 nm using a Hitachi U-3010 spectroscope equipped with an integrated sphere attachment and BaSO₄ was used as a reference. Raman spectra were recorded on a microscopic confocal Raman spectrometer (Renishaw 1000 NR) with an excitation of 514.5 nm laser light. The HPLC experiments were performed on an Waters 2695 Series LC system (Waters, Empower 3 2695-2489), which consisted of an autosampler, an online degasser, a quatpump, a thermostatted column compartment, and a fluorescence detector ($E_x = 274 \text{ nm}$, $E_m = 440 \text{ nm}$). Waters ChemStation was employed for the LC system to acquire and analyze chromatographic data. Separation was performed on a C18 column (5 μm particlesize, 150 mm \times 4.6 mm xbridge) from Waters Co., Ltd. Thermogravimetric analysis (TGA) and differential thermal analysis (DSC) were performed on a Dupont 1090 thermal analyzer. The atmosphere was air and the heating rate was 10 °C min $^{-1}$. The MS and MS/MS analysis were performed on an Agilent Q-TOF 6510 time of flight mass spectrometer.

2.5. Photocatalytic experiments

In this work, photo-degradation of organic pollutant deoxynivalenol (DON) in aqueous solution under UV (254 nm, 365 nm) light irradiation was adopted to evaluate the photocatalytic performance of the graphene/ZnO photocatalysts GZX (0.1, 0.3, 3.0, 5.0, 8.0, and 10.0). The concentration of deoxynivalenol (DON) is adjusted at 15 ppm. Before the light irradiation, a suspension of a 50 mL probe pollutants solution and 25 mg photocatalysts was stirred for 1 h under dark to reach the adsorption-desorption equilibrium. At certain time intervals, a suspension (2 mL) was extracted and centrifuged to remove the photocatalyst. The concentrations of probe pollutants were characterized by HPLC system (Waters 2695 Series, LC system Waters, Empower 3 2695-2489) with a C18 column (5 μm particlesize, 150 mm \times 4.6 mm xbridge) from Waters Co., Ltd reversed phase column.

2.6. Mass spectrometry by ESI-MS

ESI-MS studies were carried out to determine m/z values for the degraded product of DON and DON standard solution. The electron spray MS and MS/MS spectra for HPLC eluate were recorded on an Agilent Q-TOF 6510 mass spectrometer equipped with a dual electron spray ionisation source. The ESI interface was used in positive ion mode with the following settings: gas temp at 350 °C; drying gas with 10 L/min; pressure of nebulizer at 40 psig; fragmentor at 120 V; skimmer at 65 V; oCT 1 RF Vpp at 750 V; stop time about No limit/as pump Cycle Time at 0.333 s. All other source parameters were automatically tuned for maximum signal intensity of a reference solution (Agilent). The mass spectrometer was operated in a scan range from m/z 100 to m/z 1000 with a resolving

power setting of 60,000 FWHM (at m/z 400). Data were recorded using Qualitative Analysis B.07.00 and PCDL Manager B.07.00 (Agilent). For MS/MS measurements, the energy of collision-induced dissociation (10 eV; 20 eV; 40 eV) was used. The obtained m/z values were compared with the molecular weights of standard DON and its probable degraded product.

3. Results and discussion

3.1. Morphology of graphene/ZnO photocatalysts

A series of graphene/ZnO hybrid photocatalysts have been obtained by a simple hydrothermal treatment of ZnO nanoparticles and graphene oxide in water, and the typical sample were denoted as GZ0.3. This treatment process under the hydrothermal condition will easily reduce GO to GR, while simultaneously, the particles of ZnO are dispersed on the graphene sheet. Fig. 1 displays the sample digital photographs and electron microscopy images of the final solid product GZ0.3 with 0.3 wt.% weight addition of graphene. As shown in Fig. 1a, the color exhibited grey white for GZ0.3, similar phenomenon is also observed for other weight addition of graphene for GZX series materials. The morphology of the typical products was investigated by SEM and TEM. Fig. 1b and c show the SEM and TEM images of GZ0.3, from which it is seen that ZnO nanoparticles were homogeneously and tightly wrapped by graphene sheets without aggregation. The above observation further demonstrated the presence of graphene sheets helped ZnO nanoparticles from agglomeration during the growth of the graphene/ZnO hybrid, and enabled a good wrapped morphology of these oxide particles by graphene sheets.

3.2. Enhancement of photocatalytic activity

The photocatalytic activities of the graphene/ZnO hybrid, using photodegradation of DON as model reaction under UV light (365 nm), are shown in Fig. 2a and b. Fig. 2a shows the DON photodegradation rate constants on graphene/ZnO hybrid under UV light irradiation. The degradation kinetic data were fitted by using a pseudo first-order equation with a simplified Langmuir–Hinshelwood model to obtain the rate constant k [28]. The introduction of graphene into ZnO matrix drastically increased the rate constant. The photocatalytic activity trend follows the order: GZ0.3 > GZ10.0 > GZ3.0 > GZ5.0 > GZ0.1 > GZ8.0, while the sample of GZ0.3 shows the highest reaction rate constant of 0.10411 min $^{-1}$. More graphene leads to a significant decrease of photocatalytic activity. Clearly, when the weight ratio of graphene is 8.0 wt%, the activity of GZ8.0 is even lower than GZ0.1. Although graphene is beneficial for charge separation of the graphene-ZnO hybrids, it will shade ZnO at too much addition. Therefore, due to the balance between charge separation and light harvesting, the photocatalytic activity of graphene/ZnO hybrid firstly increases and then decreases with the increasing of graphene addition. As show in Fig. 2b, the rapid degradation of DON and intermediate products over the graphene/ZnO hybrid photocatalysts was clearly seen from the change of HPLC spectra of the solution in the course of the degradation. The HPLC chromatograms show increasing peaks of intermediate products at $t = 1.63 \text{ min}$, $t = 2.71 \text{ min}$ and $t = 2.97 \text{ min}$ with prolonging irradiation time, which the peak of intermediate products at $t = 1.63 \text{ min}$ to 240 min and $t = 2.97 \text{ min}$ to 15 min was disappeared, but the peak of intermediate products at $t = 2.71 \text{ min}$ was still increased with prolonging irradiation time to 300 min, indicating these three retentions times correspond to two types ($t = 1.63 \text{ min}$ and $t = 2.97$; $t = 2.71 \text{ min}$) of intermediate products. The main peak of DON at $t = 7.32 \sim 7.39 \text{ min}$ was totally disappeared with prolonging irradiation time to 15 min, which means

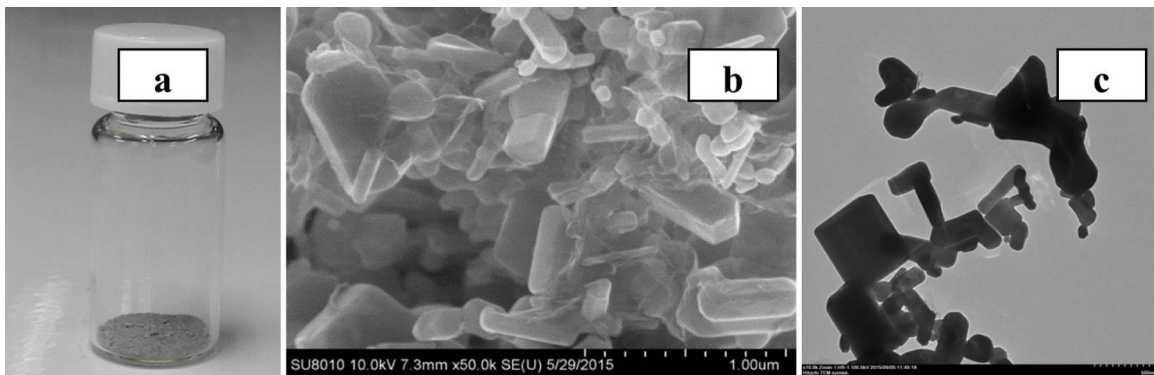


Fig. 1. Characterization of graphene-ZnO hybrid photocatalysts with 0.3 wt.% mass ratio of graphene: (a) digital photograph of GZ0.3; (b) SEM image of GZ0.3; (c) TEM image of GZ0.3.

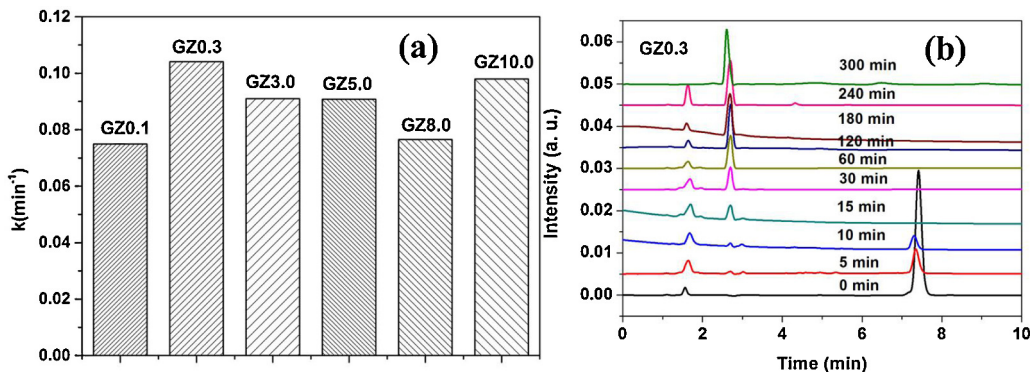


Fig. 2. (a) Apparent rate constants/curves for the photocatalytic degradation of DON over graphene-photocatalyst nanocomposites GZX series. (b) HPLC chromatograms of extension of a time about 300 min over GZ0.3 under the 365 nm irradiation.

the DON can be quickly photodegraded by graphene/ZnO hybrid GZ0.3 under UV light (365 nm).

The trend of DON and intermediate products can be obviously observed in Fig. 3a, the peak of intermediate products at $t = 2.71$ min was continuously increased and are maintain not decomposed and the other three peaks ($t = 1.63$ min, $t = 2.97$ min, $t = 7.32$ – 7.39 min) were eventually disappeared, which indicated the structure and property of intermediate products at $t = 2.71$ min could be investigated in further work. Fig. 3b shows the hybrid led to a significant photodegradation of DON in comparison with pure ZnO, traditional photocatalysts P25, g-C₃N₄ and photolysis. About 99% of the added DON (15 ppm) was degraded by graphene/ZnO hybrids within 30 min, which is 3.1 times than pure ZnO.

The way of isocratic and gradient elution for product was performed to study the amount and type of the intermediate and then definite the mechanism for photodegradation for DON further. The result was shown in Fig. 4a and b, there were three peaks ($t = 2.71$ min, $t = 3.55$ min, $t = 6.97$ min) of intermediate products appeared and the peak of intermediate products at $t = 2.71$ min was continuously increased while the other peak ($t = 3.55$ min) were eventually disappeared however the peak at $t = 6.97$ min was unchanged with prolonging irradiation time to 120 min, the products of gradient elution were consistent with the result. Based on above analysis, the DON molecule may have been degraded to small fragment molecular by ring opening and could be destroyed the fragment structure further with higher excitation energy over graphene/ZnO hybrid photocatalyst.

3.3. Structure of graphene-ZnO hybrid

The XRD patterns of the samples are shown in Fig. 5a, the broad XRD peak of the freeze-dried SGH indicates the poor order-

ing of graphene sheets along their stacking direction and reflects that the framework of the SGH is composed of few-layer stacked graphene sheets. The interlayer spacing of the freeze-dried SGH was calculated to be 3.76 Å. This value is much lower than that of GO precursor (6.94 Å) while slightly higher than that of natural graphite (3.36 Å) [29,30]. These results suggest the existence of π-π stacking between graphene sheets in the SGH and also the presence of residual oxygenated functional groups on reduced GO sheets. Thanks to these residual hydrophilic oxygenated groups, the reduced GO sheets can encapsulate ZnO in the process of hydrothermal reduction. This factor together with the π-π stacking of graphene sheets resulted in the successful construction of the graphene/ZnO hybrids. It is found that the samples (ZnO, GZ0.1, GZ3.0) present the typical XRD diffraction character of wurtzite structure according to the standardized JCPDS (36–1451) card. However, no characteristic peaks of graphene are observed for either GZ0.1 or GZ3.0 in the corresponding region, which may arise from the factors that the content of the graphene is low and that the deposited ZnO particles prevent the graphene sheets from forming the erratic stacks. The graphene/ZnO hybrid shows the similar broader diffraction peaks to the pure ZnO as prepared, which indicates that the size of ZnO particles is smaller. Furthermore, the diffraction peaks of the graphene/ZnO hybrid are unchanged compared with that of pure ZnO, which indicates that the lattice constants of ZnO have unchanged because of surface hybridization of the carbonaceous material.³¹

The FTIR spectra of graphene and graphene/ZnO hybrids are shown in Fig. 5b. Fig. 5b presents typical fingerprint groups of GO, including carboxylic species, hydroxyl species and epoxy species ($C=O$, 1734 cm⁻¹; OH deformation, 1400 cm⁻¹; the C—OH stretching, 1230 cm⁻¹; C—O—C (epoxy group) stretching, 1061 cm⁻¹; skeletal ring stretch, 1624 cm⁻¹) [32]. After hydrothermal reduc-

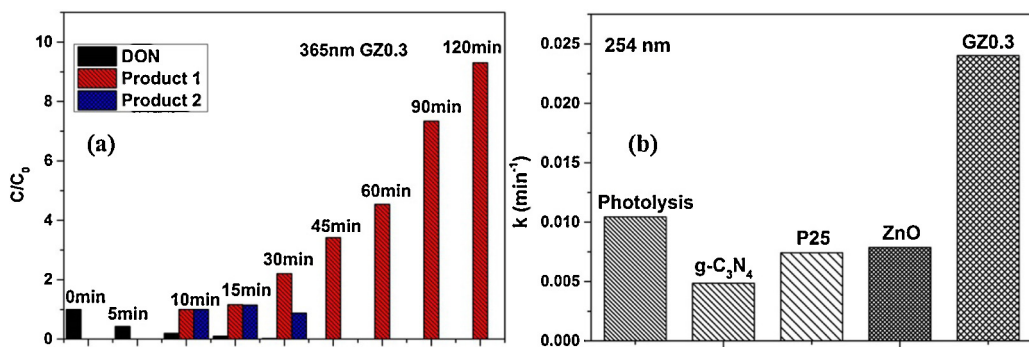


Fig. 3. Degradation rate of intermediate product over graphene/ZnO hybrid GZ0.3 under 365 nm and apparent rate constants of different photocatalysts under 254 nm for the photocatalytic degradation of DON.

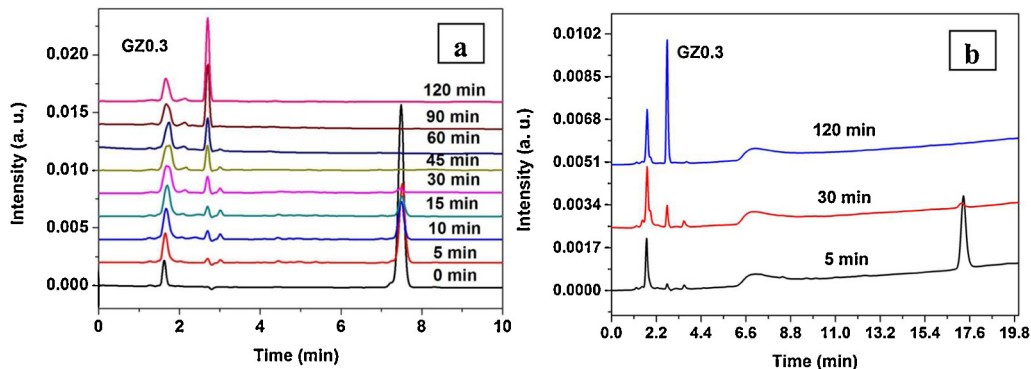


Fig. 4. Isocratic elution (a) and gradient elute (b) procedures of HPLC chromatograms for the photocatalytic degradation of DON over graphene/ZnO nanocomposites GZ0.3 under the 365 nm irradiation.

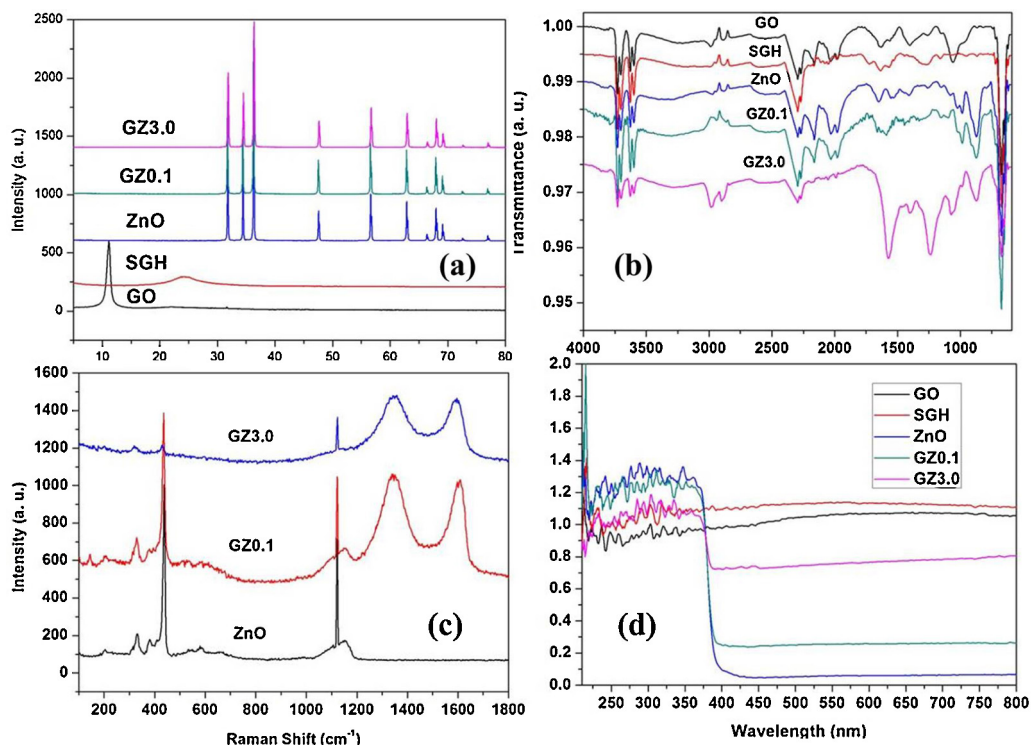


Fig. 5. Characterization of GZX series photocatalysts and blank: (a) XRD patterns; (b) FTIR spectra; (c) Raman spectrum; (d) DRS spectra.

tion, the peak of SGH (self-assembled graphene hydrogel) at 1058 cm^{-1} corresponding to the C—O—C stretching vibration decreased significantly, and the peaks at 1400 cm^{-1} attributed to

the OH deformation became relatively small [33]. The absorption characteristic band clearly shows the skeletal vibration of the graphene sheets, indicating the formation of graphene struc-

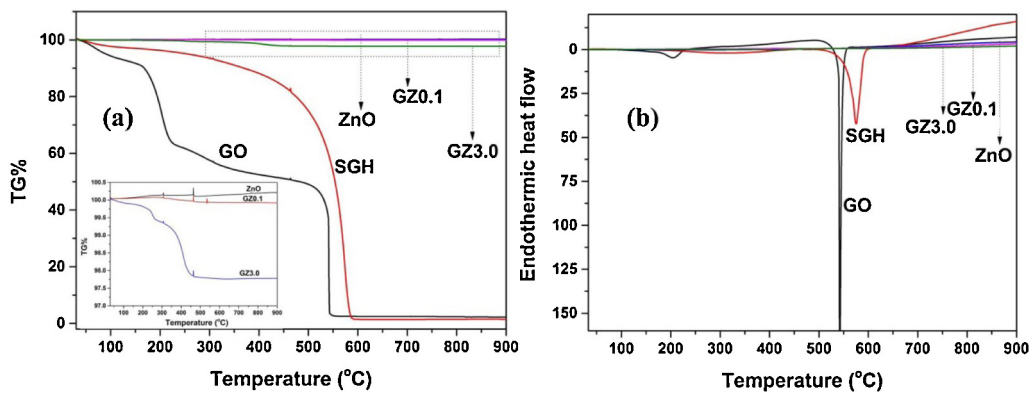


Fig. 6. (a) TGA and (b) DSC curves of graphene/ZnO photocatalysts and blank controls.

ture. The hybridization between ZnO and graphene sheets resulted in some changes in the FTIR spectrum. Compared to graphene, it can be found that many new peaks were introduced into the FTIR spectrum of graphene after hybridization. These new peaks at 1572 cm^{-1} , 1236 cm^{-1} and 1073 cm^{-1} were observed from the FTIR spectrum of GZ3.0 and appeared at significant intensities, which indicated that there existed strong chemical interaction between graphene and ZnO molecules. Furthermore, the peak located at 2164 cm^{-1} corresponding to characteristic functional group of ZnO disappeared, which can be ascribed to surface hybridization of graphene that the surface of ZnO was coated by graphene which covered the vibration signal of ZnO. Therefore, the surface hybrid structure of graphene/ZnO can be confirmed by FTIR spectrum definitely, which play a key role in enhancing the photocatalytic efficiency for DON photo-degradation.

The Raman spectra of pristine GO and graphene/ZnO hybrid are shown in Fig. 5c, from which it can be found that the GO (Fig. S1) shows the D and G bands at 1348 and 1586 cm^{-1} . The G band is attributed to all sp^2 carbon forms and provides information on the in-plane vibration of sp^2 bonded carbon atoms while the D band suggests the presence of sp^3 defects [31]. Compared with graphene, the D band was slightly red-shifted by 6 cm^{-1} of the nanocomposites while the G band showed a blue-shift of 2 cm^{-1} . These shifts in the Raman peak could be attributed to the chemical interaction between ZnO and graphene. Raman spectroscopy is also utilized to investigate the single-, bi-, and multilayer characteristics of graphene and graphene oxide layers [34]. For instance, it was shown that the G band of the single-layer graphene, located at 1592 cm^{-1} , shifts about 2 cm^{-1} into higher wavenumbers indicated more contribution of single-layer graphene sheets in the graphene/ZnO hybrid sample. In general, the I_D/I_G intensity ratio is a measure of disorder degree and average size of the sp^2 domains in graphite materials [35–37]. Hence, a higher I_D/I_G peak intensity ratio indicate more defects and disorders of the graphitized structures containing the disorders caused on the surface of the carbon platelets. Compared with graphene ($I_D/I_G = 0.92$), the increased I_D/I_G intensity ratio for GZ3.0 ($I_D/I_G = 1.02$) is observed, implies a decrease in the size of the in-plane sp^2 domains and formation of the defects and disorders on the surface of graphene. Above results are consistent with the results in FTIR characterization, revealing the reestablishment of the conjugated graphene network (sp^2 carbon).

The absorption range of light plays an important role in the photocatalysis, Fig. 5d shows the UV-vis diffuse reflectance spectroscopy (DRS) of samples, there is not too obvious red shift of ca. $20\text{--}30\text{ nm}$ in the absorption edge of GZ3.0 powder, compared to pristine ZnO. The change in the reflectance spectra at approximately 2.95 eV (419 nm) suggests that the energy band

gap of the GZ3.0 is simply associated with broad contribution from absorbance of graphene [38]. In addition, the introduction of graphene on ZnO surface induces the increased light absorption intensity in the visible region. The stronger absorption intensity in UV and visible regions for GZ3.0 than ZnO is a key factor for higher photocatalytic activity. It can also be clearly observed that ZnO with graphene coating with disorders structure showed enhanced intensity of light absorption.

TGA is an effective analytical technique to evaluate the content of the graphene in the hybrid of graphene/ZnO photocatalysts [31]. Fig. 6a shows the curves of thermal gravimetric analysis and differential thermal analysis in air atmosphere for the graphene and graphene/ZnO hybrid. The graphene oxide powders exhibited three obvious steps of mass loss: the evaporation loss of adsorbed water about at $100\text{ }^\circ\text{C}$ (about 5% of weight loss), the removal of oxygen-containing groups accompanied by the liberation of $\text{C}_x\text{H}_y\text{O}_z$ species (about 15% of weight loss), as shown in Fig. 6b, corresponding to an obvious exothermic differential scanning calorimetry (DSC) peak at $203\text{ }^\circ\text{C}$, and the combustion of carbon layers for graphene with a strong and sharp exothermic peak at $500\text{ }^\circ\text{C}$ in DSC curve. The SGH shows only one obvious steps of mass loss that has no peak of water for physical adsorption in comparison with GO, which is located at about $573\text{ }^\circ\text{C}$ due to the removal of oxygen-containing groups. However, the curve for the graphene/ZnO hybrid sample (GZ3.0) did not exhibit three such clear steps of mass loss and had a later onset of weight loss (exclude the mass loss of adsorbed water) than GO, which showed two weak exothermic peaks at $150\text{ }^\circ\text{C}$ and $350\text{ }^\circ\text{C}$, respectively. The TGA curve of GZ3.0 sample shows a dramatical mass loss at $150\text{ }^\circ\text{C}$, which is a lower decomposition temperature for oxygen group compared with GO, indicating that the thermal stability of GO is decreased after hybridized with ZnO (inserted graph in Fig. 6a). The curve of pure ZnO shows nearly no mass loss at $900\text{ }^\circ\text{C}$ because of dry and high purity for ZnO sample which with no adsorbed water and acetate group (Fig. 6b). Based on the above analysis, these results suggested that the GZ3.0 was stabilized by the coated graphene on the surface of ZnO because of the strong chemical interaction between graphene and ZnO particles, leading to delayed weight loss of graphene. According to the TGA curve, the weight content of graphene in the composite GZ3.0 was roughly evaluated to be 2.6%, which is close to the theoretical dosage of GO (3%) while there may have a few small losses that could be attributed to the effect in the process of hydrothermal reduction.

N_2 adsorption desorption measurements with Brunauer-Emmett-Teller (BET) method was used to determine the surface area of the composites and to check the possibility of interconnected pores in the nanomaterials. As shown in Fig. 7, the nonlimiting adsorption at high P/P_0 for graphene/ZnO hybrid samples is characteristic of a Type IV loop, and the overall shapes of

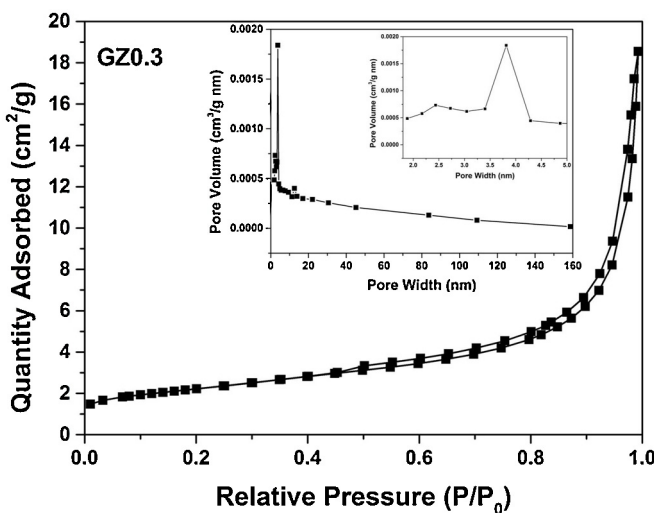


Fig. 7. N_2 adsorption–desorption isotherm and BJH pore size distribution of the graphene/ZnO hybrid photocatalyst.

Table 1

The BET surface area and pore size distribution of GZ0.3 photocatalyst and SGH sample.

Sample	S_{BET} (m^2/g)	Pore Size (nm) GZ0.3: 9.0415 SGH: 2.6408	Pore Volume (cm^3/g) GZ0.3: 0.0178 SGH: 0.2568	
GZ0.3	58.9217	85.27	9.0415	0.0178
SGH	388.9709	96.40	2.6408	0.2568

the three samples indicated their meso- and macroporous characteristics. The BET data was summarized in **Table 1**, the result analysis revealed that the graphene/ZnO hybrid had a surface area of $58.9 \text{ m}^2 \text{ g}^{-1}$, being much higher than $10.4 \text{ m}^2 \text{ g}^{-1}$ of the pure ZnO indicating that graphene is an excellent surface hybrid material for the immobilization of ZnO. The measured specific surface area ($388.9 \text{ m}^2 \text{ g}^{-1}$) and water absorption ability (96.4%) of SGH was much higher than GZ0.3 for $58.9 \text{ m}^2 \text{ g}^{-1}$ and 85.2%, respectively. In addition, the specific surface area of SGH was much less than theoretical value of an monolayer graphene sheet ($2630 \text{ m}^2 \text{ g}^{-1}$) [39], possibly because a large amount of polar groups such as hydroxyl and carboxyl on the graphene and the strong hydrogen bonding caused tight sheet associations. Thanks to these residual hydrophilic oxygenated groups, the reduced monolayer GO sheets can encapsulate ZnO in the process of hydrothermal reduction [29]. We calculated the pore-size distribution by using the Barrett–Joyner–Halenda (BJH) method from the desorption branch of the isotherm. In comparison with ZnO samples, the graphene/ZnO hybrid involved much more mesopores with the pore size centered at 3.8 nm and the average pore size located at 9.0 nm (the inset of **Fig. 7**), the pores are uniformly distributed over GZ0.3 sample. The dV/dD of GZ0.3 is about $0.01 \text{ cm}^3/\text{g}$, while is about $0.25 \text{ cm}^3/\text{g}$ for SGH, the slight decrease of dV/dD may be ascribed to monolayer graphene sheet tightening the stacking structure of the ZnO powder.

3.4. Mechanism on enhancement of photocatalytic activity and probable degradation products of DON

To reveal the photocatalytic mechanism further, **Fig. 8** shows the photodegradation of DON with the addition of hydroxyl radical scavenger (*t*BuOH) [40] and hole scavenger (EDTA-2Na) [41] under UV light irradiation. As shown in **Fig. 8**, the photocatalytic activity of GZ0.3 decreases largely by the addition of hole scavengers (EDTA-2Na), while reduces slightly with the addition of

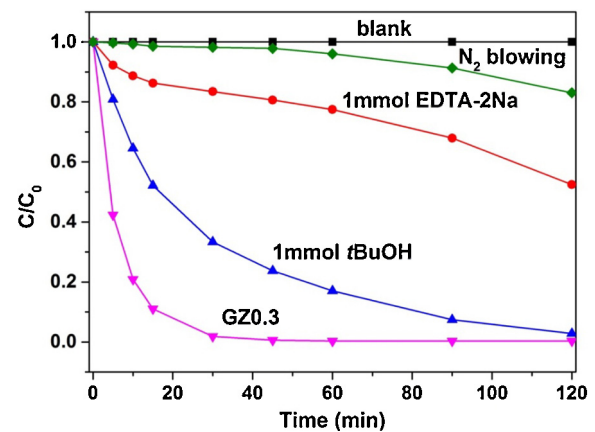


Fig. 8. Photodegradation rate curves of DON over GZ0.3 with the addition of hole, radical scavenger and N_2 under the irradiation of UV light ($\lambda = 365 \text{ nm}$).

hydroxyl radical scavengers, indicating that the hydroxyl radical are not the main oxidative species for GZ0.3 samples. That is, hole mainly plays more key role than hydroxyl radical in the UV light photocatalytic process. In addition, N_2 is also a good detective molecular to make certain the effect of O_2 , shown in **Fig. 8**. Under the anoxic suspension, the photodegraded rate of DON in GZ0.3 system is largely prohibited, indicating O_2 is even more important in the photodegradation process that produces more superoxide radicals ($\cdot\text{O}_2^-$) in comparison with the addition of *t*BuOH and EDTA-2Na system in graphene/ZnO hybrid system. Base on the above analysis, it can be concluded that the photooxidation mechanism occurring on the surface of graphene/ZnO hybrid may involve the direct oxidizing reaction of DON with superoxide radicals ($\cdot\text{O}_2^-$) and holes.

To confirm the degradation product further, the degradation products of DON under UV light were investigated and performed by ESI/MS analysis. The HPLC peak at 6.70 min of total ion chromatogram (TIC) and MS spectra in the positive ESI mode for DON are shown in **Fig. 9a** and b, which exhibits obvious enhanced photocatalytic activity for DON and appears three peaks of intermediate products under UV light irradiation. ESI/MS analysis confirmed the decreasing trend of DON and the degradation product which the secondary mass spectrogram (MS^2) in the positive ESI mode are depicted in **Fig. 10a** and b, the dominant molecular ion peak at m/z 281.8747 which is similar to that of DOM-1. Structurally, DON is a polar organic compound that belongs to the type B trichothecenes and the molecule contains three free hydroxyl groups (-OH), which are associated with its toxicity [42]. De-epoxy DON (DOM-1) is the primary metabolite produced by reduction of the 12,13-epoxygroup to a diene, which eliminated toxicity of trichothecenes by selective cleavage of their toxic 12,13-epoxy group and transformed DON into the nontoxic, de-epoxide of DON. The adduct ion for DON was found at m/z = 333.0932, which refers to DON combines with two molecules of water to form adduct $[\text{M} + \text{H}^+ + 2\text{H}_2\text{O}]^+$ and this adduct ion of DON at 333.0932 has also been reported by Razzazi-Fazeli et al. [13,43]. The other ion for DON was found at m/z = 298.8996, which may be attributed to the photo-reduction product $[\text{M} + \text{H}]^+$ of DON under UV light irradiation over graphene/ZnO hybrid. These results indicate that DON could be photodegraded rapidly in aqueous solution under UV light irradiation and may form three new degradation products. In a word, the TIC and MS^2 analysis for DON confirmed the degraded product formation and gave m/z values of 281.8747, 333.0932 and 298.8996 in positive-ion mode, suggesting that DON was reduced by photo-degradation and the new product which deduced is DOM-1, $[\text{M} + \text{H}^+ + 2\text{H}_2\text{O}]^+$, $[\text{M} + \text{H}]^+$, respectively.

On the basis of the above analysis, as shown in **Scheme 1**, it can be concluded that the enhancement of the photocatalytic

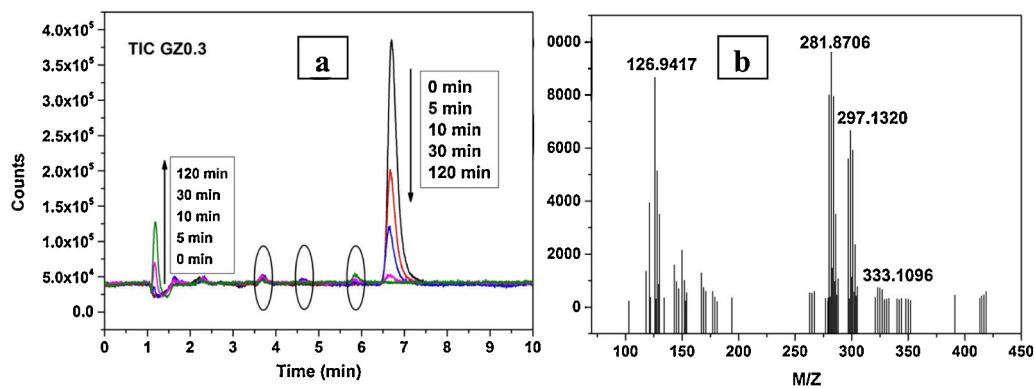


Fig. 9. Total ion chromatogram (TIC) and MS spectra in the positive ESI mode of DON over GZ0.3 photocatalyst. (a) TIC spectra; (b) MS spectra (Collision energy = 20 eV).

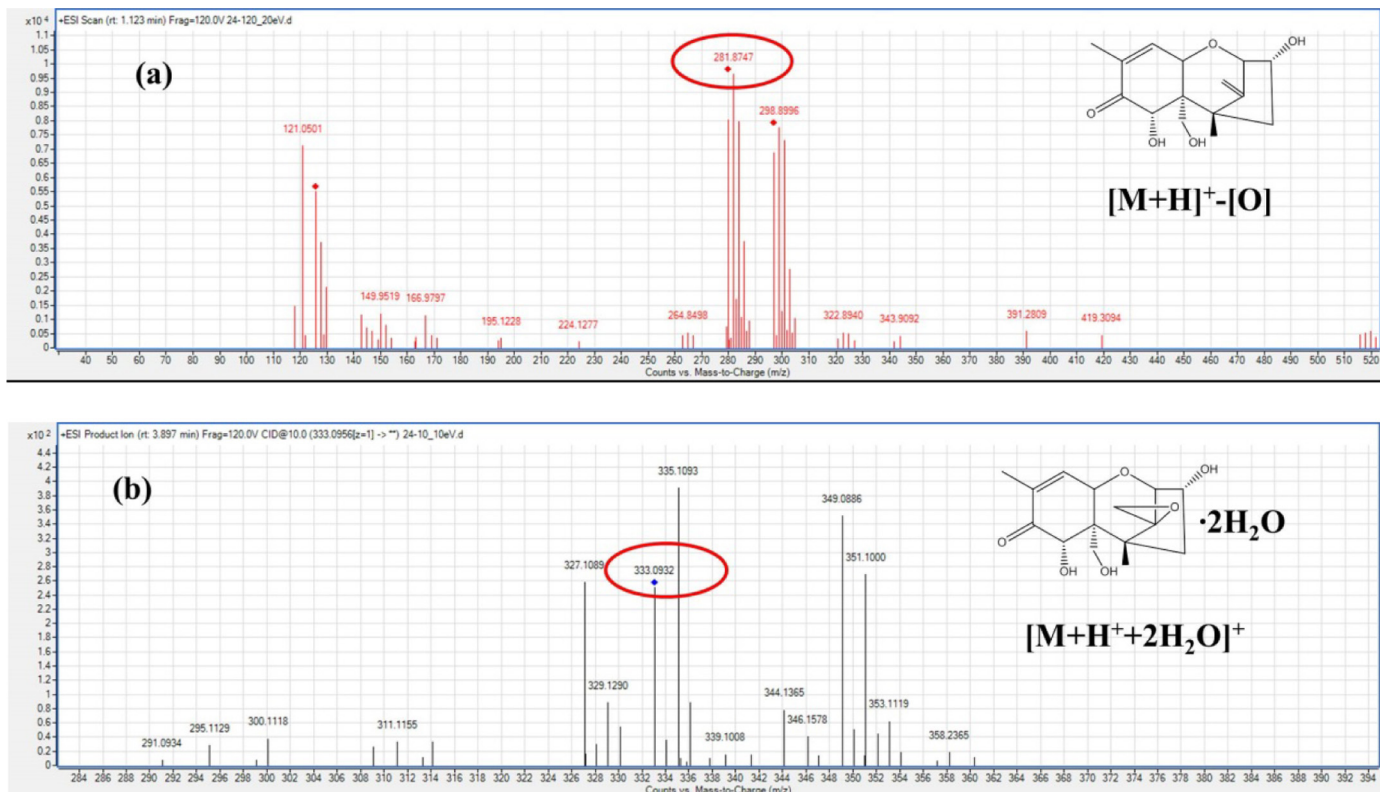
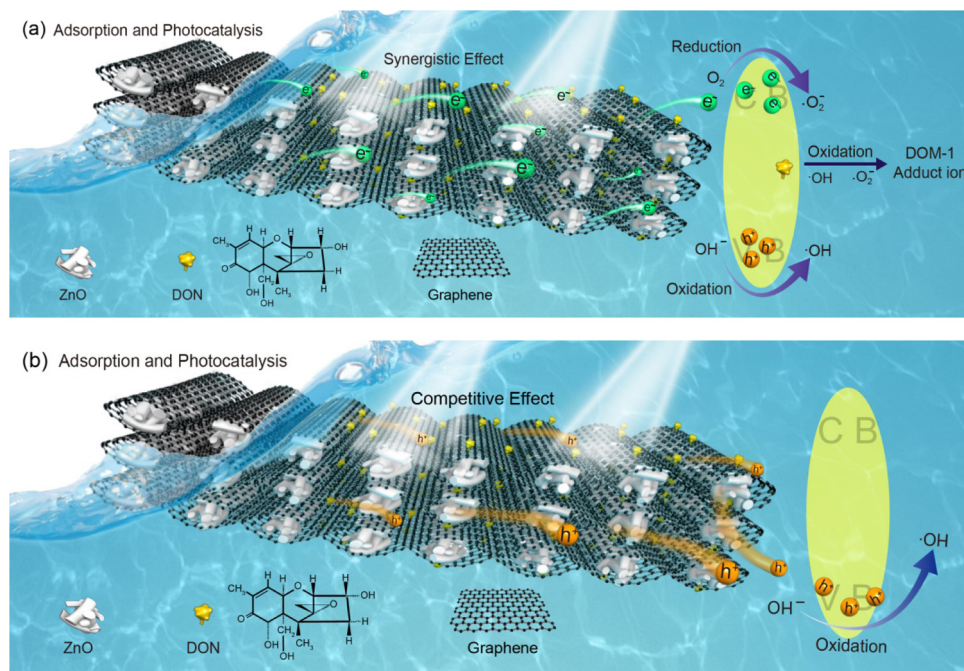


Fig. 10. The MS/MS spectra in the positive ESI mode of the degradation product for DON over GZ0.3 photocatalyst. (a) $M/Z=281.8747$; (b) $M/Z=333.0932$ (Collision energy = 20 eV).

activity of the graphene/ZnO hybrid for DON may be mainly attributed graphene which has superior electrical conductivity, enhance adsorption ability and a good hybrid layer which serve as adsorption active sites. Then a possible mechanism for the synergistic and competitive photocatalysis is proposed. As shown in Scheme 1a, it has been observed that the initial introduction of graphene into ZnO matrix drastically increased the rate constant which mainly attributed to the synergistic effect of graphene and ZnO. It was reported that graphene as electron acceptor was a competitive candidate for the electron acceptor material due to its two dimensional p-conjugation structure. We may consider that in the graphene/ZnO hybrid, the excited electrons of ZnO can quickly transfer from the conduction band of ZnO to the graphene, and then effectively suppresses the recombination of photogenerated charge carriers, leaving more charge carriers to form highly reactive species (superoxide radicals ($\cdot O_2^-$) and holes) and promote the degradation of DON molecules, the similar result have

been confirmed by Zhang et al. [20]. It is known that graphene has a high work function, which enables an easy and fast transfer of conduct band electron of ZnO, being similar to that of gold [44,45]. The photogenerated electrons have longer lifetime and higher efficiency to reduce electron acceptor once it is transferred from conduction band of ZnO to graphene and then form the superoxide radicals ($\cdot O_2^-$). As shown in Scheme 1b, the adsorption ability of graphene/ZnO hybrid is superior to photocatalytic ability while the weight ratio of graphene exceed 8.0 wt% which can probably be ascribed to the increase of specific surface as well as the adsorptive site on the graphene/ZnO hybrid. Although graphene is beneficial for charge separation of the graphene/ZnO hybrid, it will shade ZnO at too much addition while the competitive effect of adsorption and photocatalysis exceeds synergistic interaction between graphene and ZnO. The synergistic interaction means graphene provide a good adsorption site and support substrate for the deposition of DON molecules which making the graphene/ZnO



Scheme 1. Schematic drawing illustrating synthetic route and the mechanism of charge separation and adsorption-photocatalytic process over graphene/ZnO hybrid photocatalysts under UV light irradiation.

hybrid have a two-dimensional nanostructure while the competitive effect implies the photocatalytic effect is weaken along with the enhancement of adsorption which could also lead to increment of removal rate for DON. Therefore, due to the balance between charge separation and light harvesting, the photocatalytic activity of graphene/ZnO hybrid firstly increases and then decreases with the increasing of graphene addition. It is concluded that graphene exhibits advantages of adsorptive ability and ZnO shows enhancement of photocatalytic performance by graphene hybridization. The DON molecules are largely adsorbed onto graphene surface and then photodegraded by graphene/ZnO hybrid synergistically or competitively under UV irradiation. The graphene/ZnO hybrid can be considered an ideal and effective material to remove DON molecules in aqueous solution due to the synergistic or competitive effect of adsorption and photocatalysis.

4. Conclusions

In conclusion, ZnO/graphene monolayer hybrid with high photocatalytic performance has been successfully and directly prepared via a simple one-step hydrothermal method. The hybrid photocatalysts possess enhanced specific surface area, extended photoresponding range and intensive light intensity, which contribute to the superior photocatalytic activity for the photodegradation of DON under the irradiation of UV light. The UV light photocatalytic activity of ZnO/graphene hybrid GZ0.3 was 3.1 times than pure ZnO and about 99% of DON (15 ppm) could be photodegraded within 30 min totally while there were three peaks of intermediate products appeared. The ESI/MS analysis confirmed the photodegradation of DON and investigated the degradation product with the secondary mass spectrogram in the positive ESI mode, which gave m/z values of 281.8747, 333.0932 and 298.8996, suggesting that DON was reduced by photodegradation and the new product formed is DOM-1, $[M + H^+ + 2H_2O]^+$, $[M + H]^+$, respectively. The superior photocatalytic activity of the hybrid could be attributed to the direct oxidizing reaction of DON with superoxide radicals ($\cdot O_2^-$) and holes. The graphene/ZnO hybrid can be considered an ideal and effective material to remove DON molecules

in aqueous solution due to the synergistic or competitive effect of adsorption and photocatalysis. This work can provide important inspirations for developing of graphene-based photocatalysts for mycotoxin detoxification and environmental remedial applications.

Acknowledgments

This work was partly supported by Chinese National Science Foundation (21607034), National Basic Research Program of China (973 Program (2013CB127805), The National Key Technology R&D Program of China (2015BAK43B00) and Special Fund for Grain-scientific Research in the Public Interest in China (201513006).

Appendix A. Supplementary data

Supplementary data associated with this article can be found, in the online version, at <http://dx.doi.org/10.1016/j.apcatb.2016.11.010>.

References

- [1] J.J. Petska, Deoxynivalenol: toxicity, mechanisms and animal health risks, Anim. Feed Sci. Technol. 137 (2007) 283–298.
- [2] E. Numanoglu, V. Gokmen, U. Uygun, H. Koksel, Thermal degradation of deoxynivalenol during maize bread baking, Food Addit. Contam. 29 (2012) 423–430.
- [3] M. Bretz, M. Beyer, B. Cramer, A. Knecht, H.U. Humpf, Thermal degradation of the fusarium mycotoxin deoxynivalenol, J. Agric. Food Chem. 54 (2006) 6445–6451.
- [4] I. Alassane-Kpembi, M. Kolf-Clauw, T. Gauthier, R. Abrami, F.A. Abiola, I.P. Oswald, O. Puel, New insights into mycotoxin mixtures: the toxicity of low doses of type B trichothecenes on intestinal epithelial cells is synergistic, Toxicol. Appl. Pharmacol. 272 (2013) 191–198.
- [5] B. Kluger, C. Bueschl, M. Lemmens, F. Berthiller, G. Haubl, G. Jauneker, G. Adam, R. Krska, R. Schuhmacher, Stable isotopic labelling-assisted untargeted metabolic profiling reveals novel conjugates of the mycotoxin deoxynivalenol in wheat, Anal. Bioanal. Chem. 405 (2013) 5031–5036.
- [6] A. Stanic, S. Uhlig, A. Solhaug, F. Rise, A.L. Wilkins, C.O. Miles, Nucleophilic addition of thiols to deoxynivalenol, J. Agric. Food Chem. 63 (34) (2015) 7556–7566.
- [7] B.J. Park, K. Takatori, Y. Sugita-Konishi, I.H. Kim, M.H. Lee, D.W. Han, K.H. Chung, S.O. Hyun, J.C. Park, Degradation of mycotoxins using

microwave-induced argon plasma at atmospheric pressure, *Surf. Coat. Technol.* 201 (2007) 5733–5737.

[8] P.J. Van-Dyck, P. Tobback, M. Feys, H.V. Voorde, Sensitivity of aflatoxin B1 to ionizing radiation, *Appl. Environ. Microbiol.* 43 (1982) 1317–1319.

[9] H. Hooshmand, C.F. Klopferstein, Effects of gamma irradiation on mycotoxin disappearance and amino acid contents of corn, wheat, and soybeans with different moisture contents, *Plant Foods Hum. Nutr.* 47 (1995) 227–238.

[10] B.M. Youssef, S.R. Mahrous, N.H. Aziz, Effect of gamma irradiation on aflatoxin B1 production by *Aspergillus flavus* in ground beef stored at 5°C, *J. Food Saf.* 19 (1999) 231–239.

[11] F. Xie, Y.M. Ha, F. Wang, Studies on Gamma irradiation induced degradation of chloramphenicol in aqueous solution, *Chin. J. Radiat. Res. Radiat. Process.* 26 (2008) 151–156.

[12] F. Wang, F. Xie, X.F. Xue, Z.D. Wang, B. Fan, Y.M. Ha, Structure elucidation and toxicity analyses of the radiolytic products of aflatoxin B1 in methanol-water solution, *J. Hazard. Mater.* 192 (2011) 1192–1202.

[13] S. Mishra, S. Dixit, P.D. Dwivedi, H.P. Pandey, M. Das, Influence of temperature and pH on the degradation of deoxynivalenol (DON) in aqueous medium: comparative cytotoxicity of DON and degraded product, *Food Addit. Contam. Part A* 31 (2014) 121–131.

[14] Q.H. Wu, L. Lohrey, B. Cramer, Z.H. Yuan, H.U. Humpf, Impact of physicochemical parameters on the decomposition of deoxynivalenol during extrusion cooking of wheat grits, *J. Agric. Food Chem.* 59 (2011) 12480–12485.

[15] H.N. Mishra, C. Das, A review on biological control and metabolism of aflatoxin, *Crit. Rev. Food Sci. Nutr.* 43 (2003) 245–264.

[16] J.C. Young, T. Zhou, H. Yu, H. Zhu, J. Gong, Degradation of trichothecene mycotoxins by chicken intestinal microbes, *Food Chem. Toxicol.* 45 (2007) 136–143.

[17] D.S. Bhatkhande, V.G. Pangarkar, A.A. Beenackers, Photocatalytic degradation for environmental applications-a review, *J. Chem. Technol. Biotechnol.* 77 (2001) 102–116.

[18] T.G. Xu, L.W. Zhang, H.Y. Cheng, Y.F. Zhu, Significantly enhanced photocatalytic performance of ZnO via graphene hybridization and the mechanism study, *Appl. Catal. B: Environ.* 101 (2011) 382–387.

[19] C. Berger, Z. Song, X. Li, X. Wu, N. Brown, C. Naud, D. Mayou, T. Li, J. Hass, A.N. Marchenkov, E.H. Conrad, P.N. First, W.A. Heer, Electronic confinement and coherence in patterned epitaxial graphene, *Science* 312 (2006) 1191–1196.

[20] H. Zhang, X.J. Lv, Y.M. Li, Y. Wang, J.H. Li, P25-Graphene composite as a high performance photocatalyst, *ACS Nano* 4 (1) (2010) 380–386.

[21] J.L. Wu, X.P. Shen, L. Jiang, K. Wang, K.M. Chen, Solvothermal synthesis and characterization of sandwich-like graphene/ZnO nanocomposites, *Appl. Surf. Sci.* 256 (2010) 2826–2830.

[22] X.Y. Zhang, H.P. Li, X.L. Cui, Y.H. Lin, Graphene/TiO₂ nanocomposites: synthesis, characterization and application in hydrogen evolution from water photocatalytic splitting, *J. Mater. Chem.* 20 (2010) 2801–2806.

[23] G. Williams, P.V. Kamat, Graphene-semiconductor nanocomposites: excited-state interactions between ZnO nanoparticles and graphene oxide, *Langmuir* 25 (24) (2009) 13869–13873.

[24] T.N. Lambert, C.A. Chavez, B. Hernandez-Sanchez, P. Lu, N.S. Bell, A. Ambrosini, T. Friedman, T.J. Boyle, D.R. Wheeler, D.L. Huber, Synthesis and characterization of titania-graphene nanocomposites, *J. Phys. Chem. C* 113 (46) (2009) 19812–19823.

[25] K. Gouveia, F. Wypych, S.G. Moraes, N. Duran, N. Nagata, P. Peralta-Zamora, Semiconductor-assisted photocatalytic degradation of reactive dyes in aqueous solution, *Chemosphere* 40 (2000) 433–440.

[26] B. Dindar, S. Icli, Unusual photoreactivity of zinc oxide irradiated by concentrated sunlight, *J. Photochem. Photobiol. A Chem.* 140 (2001) 263–268.

[27] W.S. Hummers, R.E. Offeman, Preparation of graphitic oxide, *J. Am. Chem. Soc.* 80 (1958) (1339–1339).

[28] Y.J. Li, X.D. Li, J.W. Li, J. Yin, Photocatalytic degradation of methyl orange by TiO₂-coated activated carbon and kinetic study, *Water Res.* 40 (2006) 1119–1126.

[29] Y.X. Xu, K.X. Sheng, C. Li, G.Q. Shi, Self-assembled graphene hydrogel via a one-step hydrothermal process, *ACS Nano* 4 (2010) 4324–4330.

[30] A.V. Murugan, T. Muraliganth, A. Manthiram, Rapid, facile microwave-solvothermal synthesis of graphene nanosheets and their polyaniline nanocomposites for energy storage, *Chem. Mater.* 21 (2009) 5004–5006.

[31] D.Y. Fu, G.Y. Han, Y.Z. Chang, J. Dong, H: The synthesis and properties of ZnO-graphene nano hybrid for photodegradation of organic pollutant in water, *Mater. Chem. Phys.* 132 (2012) 673–681.

[32] J. Xu, L. Wang, Y.F. Zhu, Decontamination of bisphenol a from aqueous solution by graphene adsorption, *Langmuir* 28 (2012) 8418–8425.

[33] V. Chandra, J. Park, Y. Chun, J.W. Lee, I.C. Hwang, K.S. Kim, Water-dispersible magnetite-reduced graphene oxide composites for arsenic removal, *ACS Nano* 4 (2010) 3979–3986.

[34] D.X. Yang, A. Velamakanni, G. Bozoklu, S. Park, M. Stoller, R.D. Piner, S. Stankovich, I. Jung, D.A. Field, C.A. Ventrice, R.S. Ruoff, *Carbon* 47 (2009) 145–152.

[35] O. Akhavan, Graphene nanomesh by ZnO nanorod photocatalysts, *ACS Nano* 4 (2010) 4174–4180.

[36] C. Gomez-Navarro, R.T. Weitz, A.M. Bittner, M. Scolari, A. Mews, M. Burghard, K. Kern, Electronic transport properties of individual chemically reduced graphene oxide sheets, *Nano Lett.* 7 (2007) 3499–3503.

[37] X.J. Bai, L. Li Wang, Y.F. Zhu, Visible photocatalytic activity enhancement of ZnWO₄ by graphene hybridization, *ACS Catal.* 2 (2012) 2769–2778.

[38] X.J. Bai, L. Wang, R.L. Zong, Y.H. Lv, Y.Q. Sun, Y.F. Zhu, Performance enhancement of ZnO photocatalyst via synergic effect of surface oxygen defect and graphene hybridization, *Langmuir* 29 (2013) 3097–3105.

[39] Y. Zhu, S. Murali, W. Cai, X. Li, J.W. Suk, J.R. Potts, R.S. Ruoff, Graphene and graphene oxide: synthesis, properties, and applications, *Adv. Mater.* 22 (2010) 3906–3924.

[40] L. Hyunjoo, C. Wonyong, Photocatalytic oxidation of arsenite in TiO₂ suspension: kinetics and mechanisms, *Environ. Sci. Technol.* 36 (2002) 3872–3878.

[41] J.H. Zhou, C.Y. Deng, S.H. Si, Y. Shi, X.L. Zhao, Study on the effect of EDTA on the photocatalytic reduction of mercury onto nanocrystalline titania using quartz crystal microbalance and differential pulse voltammetry, *Electrochim. Acta* 56 (2011) 2062–2067.

[42] C.M. Nagy, S.N. Fejer, L. Berek, J. Molnar, B. Viskolcz, Hydrogen bondings in deoxynivalenol (DON) conformations-a density functional study, *J. Mol. Struct.* 726 (2005) 55–59.

[43] E. Razzaqi-Fazeli, J. Böhm, W. Luf, Determination of nivalenol and deoxynivalenol in wheat using liquid chromatography-mass spectrometry with negative ion atmospheric pressure chemical ionisation, *J. Chromatogr. A* 854 (1999) 45–55.

[44] Y. Yu, Y. Zhao, S. Ryu, L.E. Brus, K.S. Kim, P. Kim, Tuning the graphene work function by electric field effect, *Nano Lett.* 9 (10) (2009) 3430–3434.

[45] G.D. Jiang, Z.F. Lin, C. Chen, L.H. Zhu, Q. Chang, N. Wang, W. Wei, H.Q. Tang, TiO₂ nanoparticles assembled on graphene oxide nanosheets with high photocatalytic activity for removal of pollutants, *Carbon* 49 (2011) 2693–2701.